THE ASTROPHYSICAL JOURNAL, 433:797–810, 1994 October 1

GRAIN DESTRUCTION IN SHOCKS IN THE INTERSTELLAR MEDIUM

A. P. JONES,[1,2] A. G. G. M. TIELENS,[2] D. J. HOLLENBACH,[2] AND C. F. MCKEE[1]
Received 1993 September 15; accepted 1994 March 30

ABSTRACT

Destruction of interstellar dust occurs predominantly in supernova shock waves in the warm neutral/ionized medium (density $\simeq 0.25$ cm^{-3}, temperature $\simeq 10^4$ K). Recent theoretical developments and laboratory data for sputtering processes and grain-grain collisional vaporization allows us to better evaluate the grain destruction rate in interstellar shocks in the warm medium. We find that, independent of composition, grain denstruction in supernova blast waves is dominated by nonthermal sputtering for shock velocities >50 km s^{-1} and ≤ 150 km s^{-1} and thermal sputtering at higher shock velocities. We use a detailed scheme for the vaporization of grains colliding at high velocities ($v_s \geq 20$ km s^{-1}) and show that the grain-grain collision destruction process is only dominant for shock velocities of ≤ 50–80 km s^{-1} and is less important than previously assumed. Nevertheless, the grain-grain destruction rates are of order 30%–90% of the sputtering rates at 100 km s^{-1} $< v_s <$ 200 km s^{-1} and are important in vaporizing the cores of grains.

Detailed results for grain destruction as a function of grain size and composition are presented. In particular, we consider Mathis, Rumpl, & Nordsieck size distribution of silicate and carbonaceous (amorphous carbon/graphite) grains. We also present results for silicon carbide, iron, ice, and porous test particles. For carbonaceous grains we find that the fractional destruction is ≤ 0.29, and for silicate it is ≤ 0.45, for $v_s \leq 200$ km s^{-1}. We have calculated grain lifetimes, using the three-phase model of the interstellar medium, and find lifetimes of 4×10^8 yr for carbonaceous grains and 2.2×10^8 yr for silicate grains. Given that the typical stardust injection timescale is 2.5×10^9 yr, we conclude that efficient mechanisms for grain growth in the interstellar medium must exist in order that a significant fraction of the refractory elements be incorporated in dust, as observed.

Therefore, although our improved model has less vaporization of dust due to grain-grain collisions, sputtering still destroys dust efficiently and grain mantle growth in the interstellar medium is required, a conclusion reached in previous models of grain destruction in the interstellar medium.

Carbonaceous mantles on silicate grains can protect the silicate cores from sputtering destruction in interstellar shock waves, provided that the protective mantles can efficiently reform in the interstellar medium. Also, if the grains are porous the postshock grain velocities are lower than for solid particles, and grain destruction is reduced. Porosity and mantling may increase the grain lifetime by factors of ~ 3 and ~ 3–4, respectively. The fraction of interstellar silicon in silicate stardust is therefore ≤ 0.25, but more silicon might be depleted in the form of a grain mantle.

Subject headings: dust, extinction — shock waves — supernovae: general

1. INTRODUCTION

The large visual and ultraviolet extinction per H atom in the interstellar medium, the observed depletions of the grain-forming elements (i.e., C, Mg, Fe, Si, O, etc.), and the strengths of the SiO absorption features at 10 μm and 20 μm all unambiguously demonstrate that a significant proportion of the heavy elements are locked up in grains (i.e., $\geq 30\%$ for C and $\geq 90\%$ for the silicate forming elements Si, Mg, and Fe; Mathis 1990). These observed large depletions are, however, not well understood theoretically. In particular, it is well known observationally that strong shock waves efficiently destroy interstellar dust (Routly & Spitzer 1952; Cowie 1978). Theoretical estimates of shock destruction indicate grain lifetimes of the order of 10^8–10^9 yr (Barlow 1978a, b; Draine & Salpeter 1979a, b; Dwek & Scalo 1980; Seab & Shull 1983; McKee et al. 1987). In contrast, the injection timescale of newly formed dust by red giants, supernovae, and novae is much longer, $\simeq 2.5 \times 10^9$ yr (Tielens 1990). Clearly, in order to explain the observations, grains must be preserved in shocks or must efficiently grow by condensation in the cool (10–100 K), dense ($\sim 10^3$ cm^{-3}) interstellar medium.

In this paper we reconsider the destruction of grains in shocks in the light of newly derived algorithms for the destructive processes operating on the grains (Tielens et al. 1994b). We restrict our calculations to steady state shocks in the warm intercloud component of the three-phase model of the interstellar medium (McKee & Ostriker 1977); it is this component in which dominant grain destruction occurs (Seab 1987; McKee 1989). The three-phase model of the interstellar medium consists of a hot intercloud medium, warm ionized/neutral medium, or "warm intercloud medium," and the cold neutral medium, with filling factors of ~ 0.7–0.8, ~ 0.3, and ~ 0.02–0.04, mean densities of ~ 0.003 cm^{-3}, ~ 0.25 cm^{-3}, and ~ 40 cm^{-3}, and mean temperatures of $\sim 5 \times 10^5$ K, $\sim 10^4$ K, and ~ 80 K, respectively (McKee & Ostriker 1977). In the hot

[1] Department of Astronomy, University of California, Berkeley, Berkeley, CA 94720.
[2] Postal address: NASA Ames Research Center, MS 245-3, Moffett Field, CA 94035.

intercloud medium, with the largest filling factor, the densities are too low for significant destruction of grains to occur in the lifetime of a supernova remnant, and the small filling factor for the cold neutral medium (or the low frequency of high-velocity shocks) ensures that destruction in this phase contributes little to the overall grain destruction (McKee 1989). However, grains cannot be totally shielded from the destructive effects of shocks by incorporation into H I and molecular clouds, which contain $\sim 90\%$ of the mass, because gas and dust are rapidly cycled between the warm and cold phases. For example, molecular clouds are photoionized by massive star formation on timescales of the order of 3×10^7 yr (McKee 1989), and diffuse clouds are converted to warm ionized gas by photoionization in a similar timescale. In a steady state, the warm medium, which contains $\sim 10\%$ of the mass, must therefore cycle to the cold medium on timescales of the order of 3×10^6 yr. It is destruction of grains in the warm medium that determines the lifetimes of interstellar grains.

Grains subjected to interstellar shock waves undergo collisional and destructive processing due to the relative grain-grain and gas-grain motions, and the random thermal motions of the gas-phase species impinging on the grain surfaces. Differential grain velocities, due to the size and density dependence of the postshock betatron acceleration as well as the spiral motion of the charged grains around the magnetic field lines, lead to grain-grain collisions. Colliding grains may be disrupted, i.e., partially or totally vaporized, and deformed, with the degree of disruption depending on the relative velocity and collision geometry. Relative gas-grain velocities result in gas atom/ion impacts on grain surfaces, and, for a grain moving through a "stationary" gas, all atoms incident upon the grain have the same relative velocity. This destruction process, nonthermal sputtering, is dominated by helium atom/ion sputtering in a gas of cosmic composition. Thermal sputtering is important for gas temperatures in excess of 10^5 K, and in this case the relative gas-grain velocity is the thermal velocity of the gas ions. In interstellar shocks, the abundant, high-velocity hydrogen atoms/ions dominate thermal sputtering. Sputtering affects only the grain surfaces and cannot disrupt grain cores unless complete grain destruction occurs. However, grain-grain collisions that cause shattering as well as vaporization can lead to grain core disruption where the individual grain destruction is less than complete. We do not consider shattering here and therefore underestimate the destruction of the larger grains. Also we neglect the effects of the pressure drop seen in time-dependent shocks in Sedov-Taylor blast waves (McKee et al. 1987) and thereby overestimate the grain destruction. We do however estimate the effects of the pressure drop for our highest velocity shock case (200 km s^{-1}) and present the results in § 4.

In this study we are primarily concerned with amorphous carbon/graphite and silicate grains, although we also consider test particles of other interstellar, circumstellar, and dense cloud grain materials (e.g., silicon carbide, iron, and ice). We adopt the term "graphite" here for the amorphous carbon/graphite grains because we use the available graphite sputtering and vaporization parameters to model this component of interstellar dust. However, amorphous carbon has very similar sputtering and vaporization properties (Tielens et al. 1994b).

A major new conclusion of this work is that vaporization in grain-grain collisions is not an important destruction process for grains in interstellar shock waves. We find that grain destruction is dominated by sputtering processes and conclude that grain cores may be better protected from disruption than has previously been assumed. We calculate grain lifetimes that are somewhat longer than those found in previous studies (Draine & Salpeter 1979a, b; Dwek & Scalo 1980; Seab & Shull 1983; McKee et al. 1987), but still not long enough to preserve a large fraction of the grains from destruction in shocks in the interstellar medium. Thus, we are forced to conclude that grain growth must take place in the interstellar medium, or that grains have protective mantles. In a paper to follow we will discuss the effects of grain shattering in grain-grain collisions, the protection of grain cores by mantles, and the cycling of dust through the phases of the interstellar medium.

The paper is organized as follows: in § 2 the shock structure and the grain dynamics are described, § 3 details the numerical method, §§ 4 and 5 give the results of our calculations for Mathis, Rumpl, & Nordsieck (1977, hereafter MRN) size distributions and test particles, §§ 6 and 7 discuss grain lifetimes and grain growth (mantles) in the interstellar medium, and § 8 presents our conclusions.

2. SHOCK STRUCTURE AND DUST DYNAMICS

In general, the structure of an interstellar shock depends on the shock velocity v_s and on all the parameters describing the upstream state of the gas: the density n_0, the temperature T_0, the components of the magnetic field parallel and perpendicular to the shock velocity, $B_\parallel$ and $B_{0\perp}$, the abundances, and the ionization state of the gas. In these calculations, we have assumed a gas of cosmic elemental abundance consisting of H, He, O, C, N, Ne, Fe, Si, Mg, and S (Allen 1983). The fractions of these elements assumed to be in dust are O (0.16), C (0.58), Fe (0.95), Si (0.90), and Mg (0.95) (Draine & Lee 1984). The preshock ionization state of the upstream gas is given in Table 1, and the postshock ionization state is calculated self-consistently within the shock structure profiles (Raymond 1992). We consider only highly supersonic J shocks [$v_s \gg (kT_0/\mu)^{1/2}$, where μ is the mean mass per particle], so the dependence on T_0 may be neglected and the ions and neutral gas particles move as one fluid. If, in addition, the Alfvén Mach number $M_A \equiv (4\pi\rho_0 v_s^2/B_0^2)^{1/2}$ is sufficiently large, then the shock structure depends only on the normal component of the field $B_{0\perp}$. This approximation is accurate to within 30% for $M_A > 5B_\parallel/B_{0\perp}$ according to Hollenbach & McKee (1979). For typical values in the warm medium, $M_A \simeq 9.0 v_{s7}$ (with $v_{s7} = v_s/10^7$ cm s^{-1}) and this condition is likely to be satisfied. For clarity, we use B_0 to represent $B_{0\perp}$.

For the adopted abundances and ionizations, the structure of a strong shock thus depends on only three parameters, n_0, B_0, and v_s. Further simplification is possible for shocks in the diffuse interstellar medium, in which the densities are low enough that the cooling rate per unit volume scales as n^2. In this case, if the shock structure is expressed in terms of the column density behind the shock, then reference to equations (2.28) and (2.29) of Hollenbach & McKee (1979) shows that the structure depends upon only two parameters, v_s and $M_{A\perp} \equiv (4\pi\rho_0 v_s^2/B_0^2)^{1/2}$. To verify this conclusion, we have considered two 100 km s^{-1} shocks with the same value of $M_{A\perp}$, $n_0 = 0.25$ cm^{-3} with $B_0 = 3$ μG (shock 4 in Table 1) and $n_0 = 25$ cm^{-3} with $B_0 = 30$ μG (shock 7 in Table 1). Scaled by the density, the two shock structures are identical when plotted against postshock column density, and we find, as expected, that the level of grain destruction at given column density is the same in both cases. The levels of grain destruction for these shocks,

TABLE 1

SHOCK PARAMETERS AND PRESHOCK CONDITIONS

SHOCK	$M_{A\perp}$[a]	n_0 (cm^{-3})	B_0 (μG)	v_s (km s^{-1})	PRESHOCK IONIZATION STATE $n_{H^+}/n_{H(total)}$	PRESHOCK IONIZATION STATE $n_{He^+}/n_{He(total)}$	UV FLUX[b] G_0
1.....	4.5	0.25	3	50	0.01	0.01	1.08
2.....	4.5	0.25	3	50	1.00	1.00	1.14
3.....	27.1	0.25	1	100	0.50	0.25	1.81
4.....	9.0	0.25	3	100	0.50	0.25	1.77
5.....	28.6	2.5	3	100	0.50	0.25	9.21
6.....	90.4	25.0	3	100	0.50	0.25	86.99
7.....	9.0	25.0	30	100	0.50	0.25	79.30
8.....	13.6	0.25	3	150	1.00	1.00	2.42
9.....	18.1	0.25	3	200	1.00	1.00	3.51

[a] Alfvén Mach number perpendicular to the velocity vector.

[b] UV photon flux term, G_0 (McKee et al. 1987, eq. [5.9]), is the total flux (shock generated plus interstellar) normalized to that of the interstellar radiation field; i.e., $G_0 = 1 + (F_{UV,shock}/F_{UV,IS})$, where $F_{UV,shock}$ and $F_{UV,IS}$ are the shock generated and interstellar UV fluxes, respectively.

presented in Table 2, show a small difference which is attributable to a small discrepancy in the scaling of the ultraviolet photon fluxes in the shock profile data.

The degree of destruction for a given grain material is dependent upon the relative gas-grain and grain-grain velocity; the higher the relative velocity, the greater the grain destruction. We have adopted the grain dynamics of McKee et al. (1987) in our calculation of the relative gas-grain postshock velocities. In the frame of reference of the shocked gas, the grains cross the shock plane with three-quarters of the shock velocity, are betatron accelerated, and gyrate perpendicular to the magnetic field $\boldsymbol{B}$.

The interaction between the grain and the magnetic field is mediated by the grain charge. For the grain charge we use the analytical scheme of McKee et al. (1987) and find that the graphite and silicate grain charges are essentially identical. The betatron acceleration of the grains occurs mostly in the cooling postshock gas where the compressing gas produces an increasing $\boldsymbol{B}$ field which accelerates the charged grains with respect to the gas. However, collisional and plasma drag forces between the gas and drifting grains try to bring the grains to rest with respect to the gas. The deceleration produced by the drag is proportional to the grain area and inversely proportional to the grain mass and therefore varies as $(a\rho_{gr})^{-1}$, where a is the grain radius and ρ_{gr} is the material density of the grain. Therefore, small and low-density grains are least likely to be betatron accelerated and will be the most resistant to destruction in shocks.

TABLE 2

PERCENTAGE GRAPHITE/SILICATE DESTRUCTION BY MASS

MODEL	v_s (km s^{-1}) 50	100	150	200
$B_0 = 3\ \mu$G:				
$n_0 = 0.25\ cm^{-3}$	1.5/2.0	11.3/22.3	20.4/39.9	28.5/44.5
$n_0 = 2.5\ cm^{-3}$	...	18.7/36.9	...	...
$n_0 = 25\ cm^{-3}$	...	26.2/50.3	...	...
$B_0 = 1\ \mu$G:				
$n_0 = 0.25\ cm^{-3}$	...	19.1/37.6	...	...
$B_0 = 30\ \mu$G:				
$n_0 = 25\ cm^{-3}$	...	10.6/21.2	...	...
$B_0 = 3\ \mu$G:				
$n_0 = 0.25\ cm^{-3}$ ..... (fully ionized preshock)	1.1/1.6	...	...	...

3. NUMERICAL MODEL

The shock theory of McKee et al. (1987) and a more refined treatment of the grain destructive processes (Tielens et al. 1994b) have been implemented in a new code for the time-dependent treatment of grain destruction in shock waves. The numerical code integrates 72 simultaneous differential equations through a fixed shock profile and includes the grain velocity and total mass equations for each of the 18 mass bins for two grain types.

The algorithm used here to model the mass-loss processes operating on grains in interstellar shock waves is based on the grain coagulation model of Nakagawa, Nakagawa, & Hayashi (1981) and Mizuno, Markiewicz, & Völk (1988). This method strictly guarantees the conservation of mass and is described in greater detail in Appendix A. The processes that we model are thermal and nonthermal sputtering and the vaporization of grains upon collision with other grains (Tielens et al. 1994b). Previous treatments (Seab & Shull 1983; McKee et al. 1987) crudely incorporated grain-grain collisions with a simple "all or nothing" energy argument. In these treatments the grains in the collision were totally vaporized if the collision was above a threshold energy; however, there was no vaporization below this critical energy. As discussed in Tielens et al. (1994b), we include partial vaporization by lower energy collisions and make better estimates of the energy needed for total vaporization. The net effect is a lowering of the amount of vaporization by grain-grain collisions in a given shock. The grain material vaporization and sputtering parameters used in the calculation are given in Table 3.

In the calculation we assume an initial MRN power-law size distribution, where the grain number density per unit mass $dn_{gr}(m)/dm$ is given, $dn_{gr}(m) = D_i n_H m^{-\beta} dm$ ($\beta = 11/6$, $D_{graphite} = 1.50 \times 10^{-27}$ $g^{5/6}$ per H nucleus and $D_{silicate} = 2.21 \times 10^{27}$ $g^{5/6}$ per H nucleus). This distribution is often given in units of number density per unit radius, $dn_{gr}(a)/da \propto a^{-3.5}$. The total grain masses ($M_{graphite} = 5.6 \times 10^{-27}$ g per H nucleus and $M_{silicate} = 8.8 \times 10^{-27}$ g per H nucleus) are distributed across z logarithmically defined mass bins for each grain material (upper mass limit m_+ and lower mass limit m_-), where the bin upper mass limits are m_1 ($\equiv m_+$), m_2, m_3, ..., m_k ($\equiv m_+ \eta^{k-1}$), ..., m_- ($\equiv m_+ \eta^z$). The factor η is the logarithmic

TABLE 3

GRAIN MATERIAL VAPORIZATION AND SPUTTERING PARAMETERS

Parameter	Carbon	Silicate	SiC	Iron	Icy Material
ρ_0 (g cm^{-3})	2.2	3.3	3.1	7.9	1.0
C_0 (km s^{-1})	1.8	5.0	7.7	4.1	2.0
s	1.9	1.23	1.1	1.5	1.4
ϵ_V ($\times 10^{11}$ erg g^{-1})	6.4	4.8	8.1	1.4	0.54
P_t ($\times 10^{12}$ dyne cm^{-2})	5.8	5.4	8.6	5.2	0.092
V_t (km s^{-1})	23	19	25	11	6.5
U_0 (eV)	4.0	5.7	6.3	4.1	0.53
M (amu)	12	23	20	56	18
Z	6	11	10	26	10
K	0.65	0.1	0.3	0.35	0.1

NOTES.—ρ_0: specific mass density. C_0: sound speed in the solid. s: vaporization parameter. ϵ_V: vaporization energy density. P_t: vaporization threshold pressure. V_t: vaporization threshold velocity. U_0: surface binding energy. M: sputtered species atomic mass. Z: sputtered species atomic number. K: sputtering free parameter.

mass binning interval; for $\eta = 0.50$ it takes 17 mass bins to cover the MRN distribution from 50 Å to 2500 Å. An initially empty, extra bin is included at the lowest mass end of the MRN distribution. In essence, we employ a Eulerian numerical method where the bin mass "coordinates" are kept fixed and the grains are flowing through due to the destructive processes. The computational algorithm used fully accounts for the transfer of grains across bin boundaries and between bins widely separated in mass (i.e., nonadjacent bins, $\Delta k > 1$).

For each bin and for grains of a given composition, we determine as a function of time the mass power-law index across the bin (β_k), the mean grain radius ($\bar{a}_k$) and mass ($\bar{m}_k$), the total bin mass (M_k), and the mass density [$\rho_k = \bar{m}_k n(\bar{m}_k)$]. In addition we solve for the velocity of grains of mass $\bar{m}_k$, using the grain velocity equations (3.7)–(3.13) and the grain electrical potential equations (5.9)–(5.11) from McKee et al. (1987).

In this work we have not attempted to concurrently solve the shock dynamics and grain physics, but have instead adopted an approach that divorces the two. We have used shock profiles (density, temperature, electron abundance, ionization structure, and photon flux) provided by Raymond (1992) and have considered the grain destructive processes as a function of these fixed profiles. The relevant shock parameters are given in Table 1. We have assumed preshock ionization levels of 0.5 and 0.25 for H and He, respectively, for $v_s = 100$ km s^{-1}. For $v_s \geq 150$ km s^{-1}, the shock-generated ultraviolet flux is sufficient to preionize the gas, and we therefore assume a completely ionized preshock gas. In our calculation we make no allowance for any grain destruction feedback into the shock structure, such as the addition of coolants to the gas from the vaporization of grain material. This assumption is reasonable for the levels of grain destruction that we find (less than 50%) for all the radiative shocks studied (shock velocities, $v_s \leq 150$ km s^{-1}). In addition, most of the cooling in the postshock gas is due to elements with little or no depletion, e.g., H, He, and O. Therefore, the increase in heavy-element gas-phase abundances due to grain destruction does not significantly affect the shock structure. We have chosen as a "standard" shock the case for $n_0 = 0.25$ cm^{-3}, $n_e = 0.13$ cm^{-3}, $v_s = 100$ km s^{-1}, and $B_0 = 3$ μG (shock 4 in Table 1). The preshock density and magnetic field are taken as being typical of the warm component of the interstellar medium, the phase in which the dominant grain destruction occurs. The 50% ionization is an approximation to the precursor ionization caused by the shock, not the ionization state of the ambient gas. The 100 km s^{-1} shock velocity is selected as close to the optimum of the shock frequency and destructive potential for interstellar shock waves (Draine & Salpeter 1979a, b).

We have subjected our computer code to comprehensive series of tests in order to check the mass conservation and the accuracy of the results. For simple cases (i.e., fixed vaporization fraction and sputtering yield) the results of the code have been compared with analytical calculations and an exact correspondence is found. We have also checked the mass conservation by running the code for sputtering yields of zero and no fractional vaporization upon collision, and within the computational errors find that the bin masses are entirely stable. We have also run the code with identical grain components distributed over the two distinct sets of mass bins. In that case, we also find the exact same result for double that grain component mass using only one set of mass bins. Finally, we have performed test particle calculations (see § 5) in which we follow the evolution of individual grains through the shock profiles and find that results for the individual test grains are identical with those for the same size grains in the power-law mass distribution. We are therefore confident in the robustness of our computational scheme.

Interestingly, we find that very coarse mass bin calculations (with six mass bins for each grain component) give results that generally agree to $\pm 2\%$ with the 18 mass bin calculations and are an order of magnitude faster to compute.

4. RESULTS AND DISCUSSION

We have numerically calculated the graphite and silicate grain destruction for all the shocks defined in Table 1, which includes shocks with initial velocities of 50, 100, 150, and 200 km s^{-1} and a range of preshock densities and magnetic fields. The results of these calculations presented in Table 2 are similar to the results of McKee et al. (1987). However, there are both quantitative and qualitative differences between these two sets of results, and we discuss these below.

Figure 1 shows the temperature, density, and electron abundance (relative to hydrogen nuclei) profiles of our "standard" shock ($v_s = 100$ km s^{-1} and $M_{A\perp} = 9.0$, corresponding to $n_0 = 0.25$ cm^{-3} and $B_0 = 3$ μG), and Figure 2 shows the silicate grain velocities for this shock calculated using equation (A5) in Appendix A. The grain velocities are particularly important because the degree of grain destruction is primarily governed by the velocity. Figure 2 clearly shows the two regions of strong acceleration, one just behind the shock front, $N_H = 10^{14}$–10^{15} cm^{-2}, where the gas is rapidly ionized and a second prior to recombination of the gas at $T \sim 10^4$ K, $N_H = 10^{16}$–10^{17} cm^{-2}. In both regions, the rapid cooling of the gas causes a rapid rise in the gas density (see Fig. 1) and magnetic field, and the changing $\boldsymbol{B}$ field accelerates the charged grains. For a fully ionized preshock gas the initial postshock betatron acceleration associated with the ionization is absent.

In Figures 3*a* and 3*b* we present the fractional destruction rate (fraction of the total grain mass destroyed per year) and the destruction rate multiplied by time as a function of shocked column density for $v_s = 100$ km s^{-1} for grain-grain collisions and the sputtering processes. The flow time is given by $t = N_H/n_0 v_s$ and, for Figures 1–3, we have $\log t(\mathrm{yr}) = \log N_H - 13.90$, which corresponds to a time of $\sim 10^5$ yr for grains to pass through the warm ($T > 100$ K) regions of the shock. Silicate grains are mostly destroyed by nonthermal sputtering at a postshock column of $N_H \sim 10^{17}$–10^{18} cm^{-2} (where the tem-

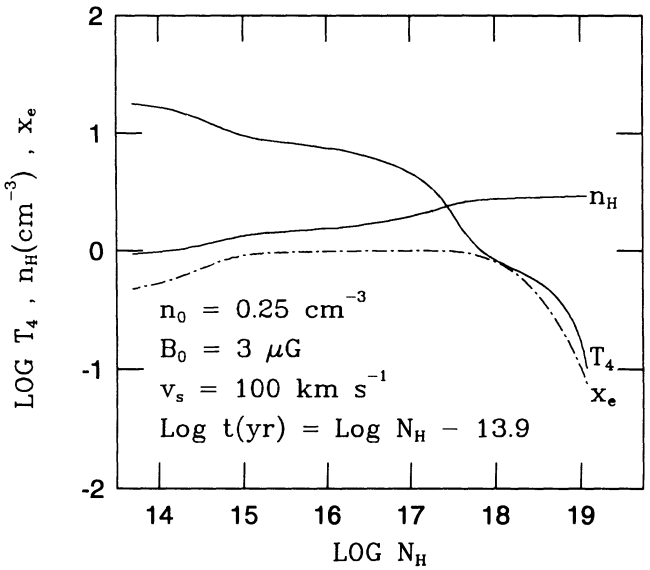

FIG. 1

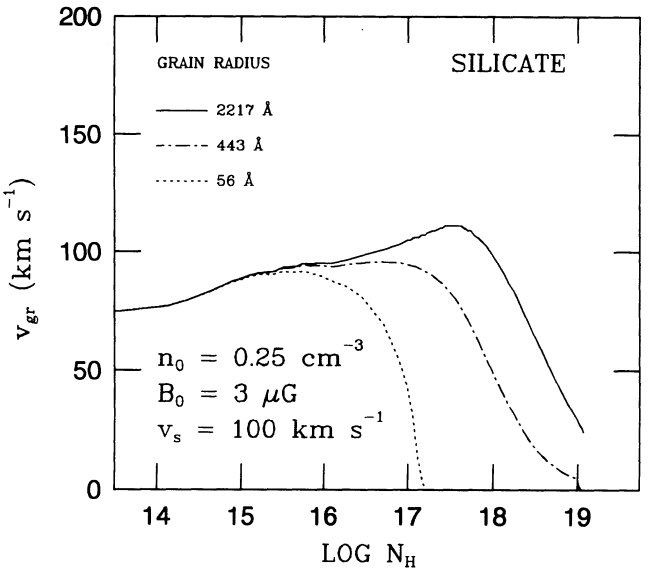

FIG. 2

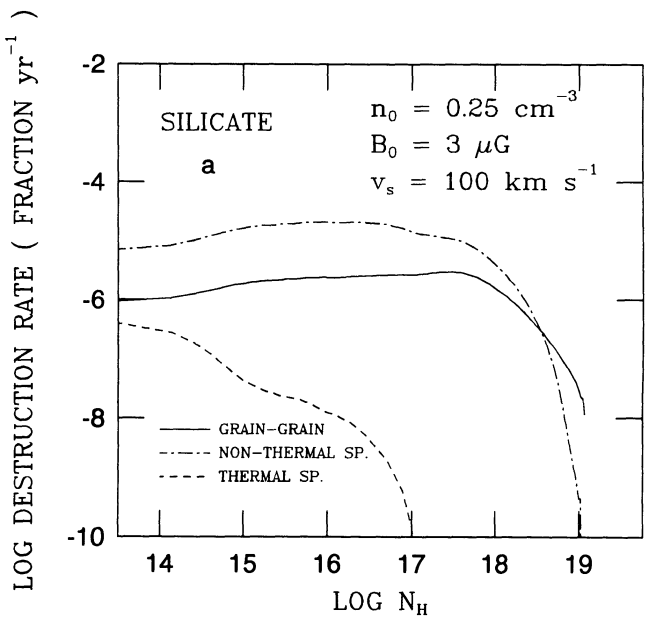

FIG. 3*a*

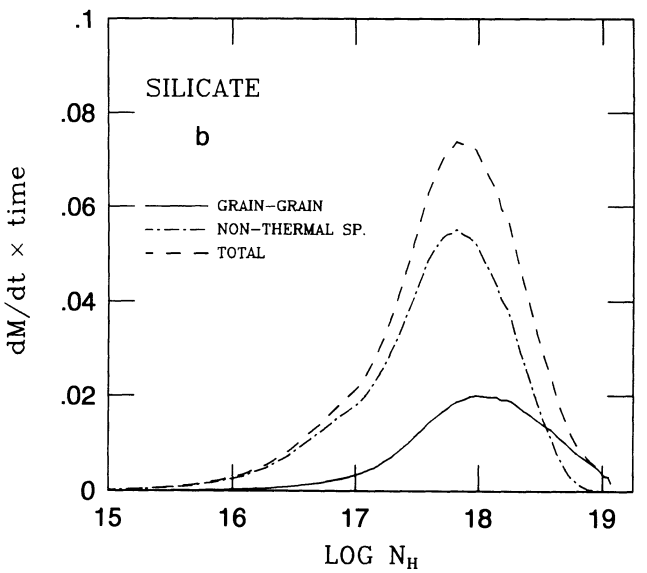

FIG. 3*b*

FIG. 1.—100 km s^{-1} shock profile [temperature, $T_4 = (T_k/10^4$ K), density, n_H, and electron relative abundance, x_e] as a function of the shocked column density for $M_{A\perp} = 9.0$ (corresponding to $n_0 = 0.25$ cm^{-3} and $B_0 = 3$ μG). To convert column density ($N_H = n_0 v_s t$) to time: log t(yr) = log N_H(cm^{-2}) − 13.9.

FIG. 2.—Silicate grain velocity as a function of shocked column density for three representative grain radii.

FIG. 3.—(*a*) Time-dependent silicate grain destruction rate (fraction destroyed per year) as a function of the shocked column density for collisional and sputtering destructive processes. (*b*) Total silicate grain destruction rate multiplied by time and plotted as a function of the logarithm of the shocked column density for collisional and sputtering destructive processes. This plot has been constructed so that equal areas show equal destruction, and clearly indicates that the grain destruction peaks near a shocked column of $N_H = 10^{18}$ cm^{-2}.

perature is dropping rapidly to 10^4 K). Note that Figure 3*a* represents a rate which needs to be multiplied by a time ($\propto N_H$) to obtain the fraction destroyed. In Figure 3*b* we plot the silicate grain destruction as dM/dt × time in order to highlight the peak in the grain destruction as a function of the shocked column of the gas; this shows that the destruction due to grain-grain collisions and nonthermal sputtering peaks at $N_H \sim 10^{18}$ cm^{-2}.

Figures 4*a*, 4*b*, and 4*c* show the grain destruction as a function of size for $v_s = 50$, 100, and 200 km s^{-1}, respectively. Our results are similar to those of McKee et al. (1987) for silicate grains subjected to a 100 km s^{-1} shock wave. However, use of the partial vaporization scheme developed by Tielens et al. (1994b), reduces the collisional destruction of the largest grains ($a > 500$ Å) by a factor of 20. The simpler approach adopted by Seab & Shull (1983) and McKee et al. (1987), i.e., total vaporization of one or both collision partners above a relatively low threshold leads to an overestimate of the destruction of the

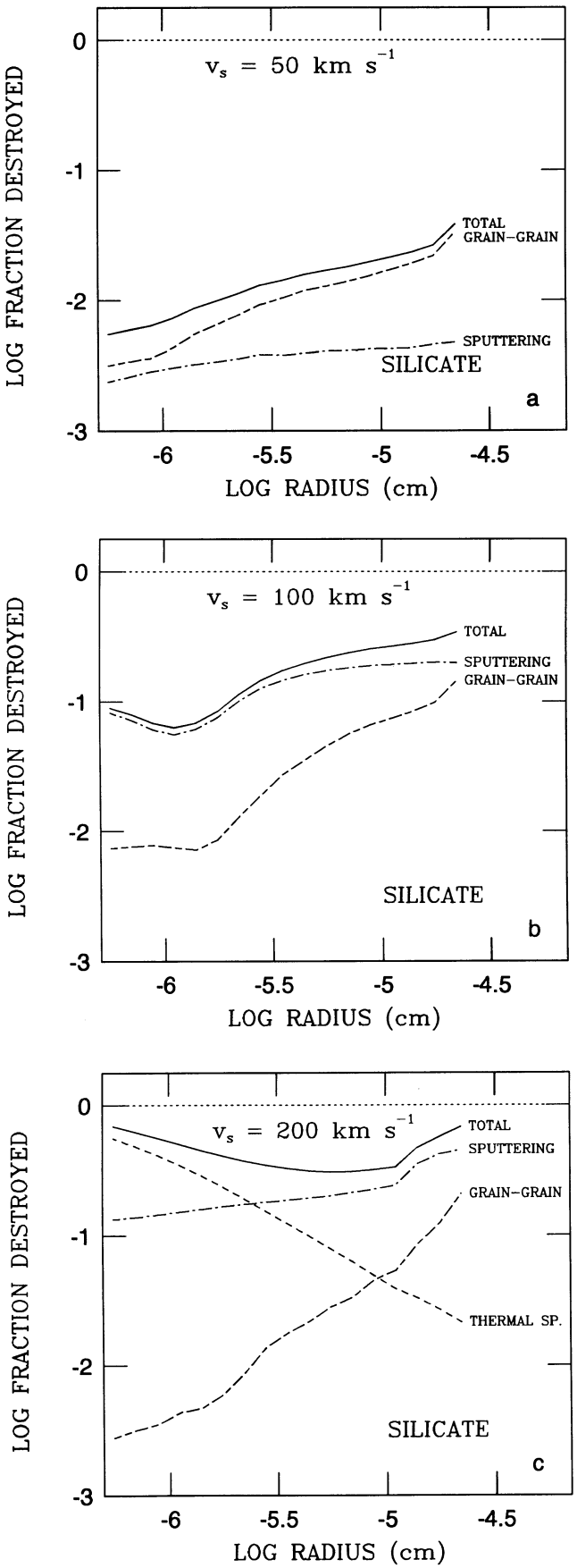

larger grains in grain-grain collisions. The small grain ($a < 500$ Å) destruction in grain-grain collisions is increased by about a factor of 2 compared to the results of McKee et al. (1987).

The grains undergo betatron acceleration and the enhanced gas-grain relative motion makes nonthermal sputtering the dominant grain destruction mechanism for 50 km s^{-1} $< v_s \leq$ 150 km s^{-1}. Our results indicate a somewhat higher destruction rate for nonthermal sputtering of silicate grains than the McKee et al. (1987) data. This is due to the improved sputtering yield expression used here (Tielens et al. 1994b) and arises because of the difference in the maxima and thresholds of the adopted silicate sputtering yields. The Tielens et al. expressions have been derived semiempirically and agree with a large body of recent experimental data. The destruction rates of small grains are sensitive to the assumed sputtering threshold values because the effects of changing the threshold are most pronounced at the lowest relative velocities, i.e., for the low-velocity small grains. The new sputtering yield increases the destruction of small grains ($a < 500$ Å), by a factor of ~ 5 for $a = 500$ Å and a factor of ~ 15 for $a = 100$ Å, while hardly affecting the sputtering destruction of the larger grains (comparison here is with the Model A, $B_0 = 3$ μG, $v_s = 100$ km s^{-1}, shock of McKee et al. 1987). This arises because the new nonthermal sputtering yields for both graphite and silicate are higher at the lower velocities. For silicate the yields are a factor of 2 higher at 100 km s^{-1} and an order of magnitude higher at 50 km s^{-1}. Hence, the nonthermal sputtering destruction for the lower velocity small grains is much higher than that of McKee et al. (1987). Note that at shock velocities ≤ 50 km s^{-1}, grain-grain collisional processes rather than sputtering dominate the total grain destruction (Fig. 5).

If the Alfvén Mach number is higher than our standard 100 km s^{-1} case (e.g., $N_{A\perp} = 27.1$, corresponding to $B_0 = 1$ μG and $n_0 = 0.25$ cm^{-3}, shock 3 in Table 1), then the grain destruction is increased by a factor of ≈ 2 (see Table 2). This effect is due to the increased postshock compression (i.e., betatron acceleration), and the resulting increase in the maximum grain velocities behind the shock by factors of ~ 1.2–1.4 for $a > 200$ Å, with the largest grains showing the largest velocity enhancements.

The overall results of these calculations for all shock velocities, and preshock densities and magnetic fields are shown in Figures 5 and 6, where the grain destruction is given as a function of grain type, shock velocity, preshock density, and the parameter $b = B_0 n_0^{-1/2}$, where B_0 is in microgauss and n_0 in cm^{-3}. The Alfvén Mach number is related to b by $M_{A\perp} = 54.2 v_{s7}/b$. It is clearly apparent from these figures and the data in Table 2 that the silicate grain destruction is enhanced over that for the graphite grains; in the 100 km s^{-1} and 150 km s^{-1} shock cases the difference is a factor of 2. This difference results from the higher grain velocities in combination with the higher nonthermal sputtering yield for the silicate grains. The larger silicate grain velocities arise from the greater betatron acceleration they experience due to their higher specific mass density. The lesser difference in the levels of graphite and silicate grain destruction at the lower shock velocities is due to the dominance of collisional destruction over sputtering. At $v_s = 200$ km s^{-1}, the overall grain destruction is more equitable because of

FIG. 4.—Postshock fractional silicate grain destruction as a function of radius, nonthermal sputtering (*dash-dotted*), thermal sputtering (*short-dashed*), and grain-grain collisional vaporization (*long-dash–short-dashed*), for $v_s =$ (*a*) 50, (*b*) 100, and (*c*) 200 km s^{-1}.

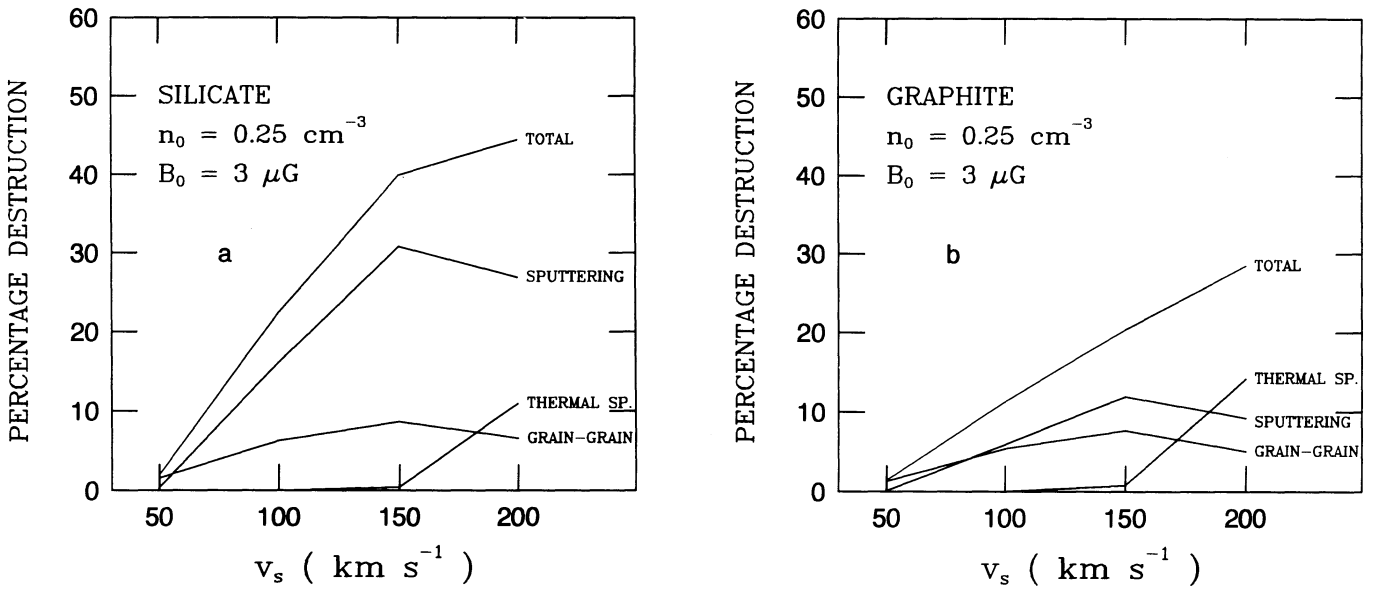

FIG. 5.—Postshock silicate grain destruction as a function of shock velocity and destructive process ("sputtering" refers to nonthermal sputtering and "thermal sp." to thermal sputtering) for fixed preshock density ($n_0 = 0.25$ cm^{-3}) and magnetic field ($B_0 = 3$ μG). (*b*) Same as (*a*), but for graphite grains.

the leveling effects of thermal sputtering (cf. Fig. 5), the graphite grains being more susceptible to thermal sputtering than the silicate grains for $T_k > 6.3 \times 10^5$ K (Tielens et al. 1994b). Some indication of this effect is to be seen in Figures 5*a* and 5*b*, where the changes in slope at high shock velocity of the total destruction are in the opposite senses for the two grain materials.

We also note from Figure 5 that the nonthermal sputtering contributions are reduced for the highest velocity case. Radiative cooling is less efficient in the 200 km s^{-1} shock, and the grains stop (relative to the gas) before the gas cools and compresses, and before the grains can betatron accelerate. Hence, for the $v_s = 200$ km s^{-1} case, the grains merely undergo deceleration from their initial relative velocity of $(3/4)v_s = 150$ km s^{-1}. In contrast, in the $v_s = 150$ km s^{-1} shock, the grains are betatron accelerated to velocities well in excess of their initial relative velocities of 112 km s^{-1}, e.g., $\sim$170 km s^{-1} in the case of the largest silicate grains.

For the 200 km s^{-1} shock case we have investigated the effects of the pressure drop that occurs in Sedov-Taylor waves, this effect is otherwise neglected in this paper but has been dealt with in detail by McKee et al. (1987). In order to investigate the pressure drop effect, we have derived an explicit expression for the pressure of an element of gas hit by a shock. From this we derive a 200 km s^{-1} shock density and temperature profile, assuming that the ionization is frozen and that there are no radiative losses. Appendix B gives full details of the profile calculation. We compare the grain destruction results for this shock with those for the case where no pressure drop is included (shock 9 in Table 1) and find that the overall grain destruction is reduced by 13% for the graphite grains and 34% for the silicate grains. These differences are entirely due to a decrease in the large-grain ($a \geq 1000$ Å) destruction by factors of 1.6 for graphite grains and 2.5 for the silicate grains. For grains smaller than 1000 Å in radius, the degree of destruction is not affected by the inclusion of the pressure drop effect. Thus, in our 200 km s^{-1} calculation where we ignore the effects of a pressure drop, we have probably overestimated the large-grain destruction by a factor of $\approx$2, and the overall grain destruction by a factor of 1.1 for graphite and 1.5 for silicate.

There is essentially no difference in the levels of grain-grain collisional destruction between graphite and silicates, as a comparison of Figures 5*a* and 5*b* attests. This reflects the comparable collisional vaporization parameters of the two grain materials; the slight enhancement in silicate grain collisional destruction is due to their higher velocities.

We note from Figure 5 that the grain-grain collisional destruction of grains does not increase dramatically with shock velocity, in contrast to nonthermal sputtering. The increased importance of sputtering, at the higher shock velocities, relative to grain-grain collisions is due to the high threshold energy for sputtering which causes the sputtering to be a stronger function of relative velocity than the vaporization by grain-grain collisions. For example, for collisions between grains of radii 400 Å and 2000 Å at 100 km s^{-1} the fractional vaporization is proportional to $v_s^{1.2}$, whereas for nonthermal sputtering the yield is proportional to $v_s^{1.8}$ (Tielens et al. 1994b, §§ 3.3 and 4.1).

Figure 6*a* shows the effects of preshock gas density on grain destruction, for fixed v_s and B_0. The degree of grain destruction increases by factors of $\sim$1.7 and $\sim$2.3 for gas density increases of one and two orders of magnitude, respectively. The column of shocked ($T > 10^4$ K) material is constant, but the betatron acceleration of the grains increases with gas density, and, hence, the level of grain destruction increases with the preshock density. In Figure 6*b* we show the level of grain destruction as a function of the parameter $b = B_0 n_0^{-1/2}$, which is proportional to the inverse of the Alfvén Mach number, $M_A^{-1} \propto B_0 n_0^{-1/2} v_s$, at constant velocity. The degree of grain destruction increases with increasing Alfvén Mach number. In other words, in shocks with high b (low $M_{A\perp}$) the postshock magnetic field reduces the gas compression, which reduces the betatron acceleration and hence the grain destruction.

In this study we have included the effects of the preshock ionization state for the lowest velocity shocks in order to compare the effects of low-velocity shocks propagating into the warm neutral medium (WNM) and the warm ionized medium (WIM) (shocks 1 and 2 in Table 1, respectively). In the WNM case, the postshock compression occurs an order of magnitude

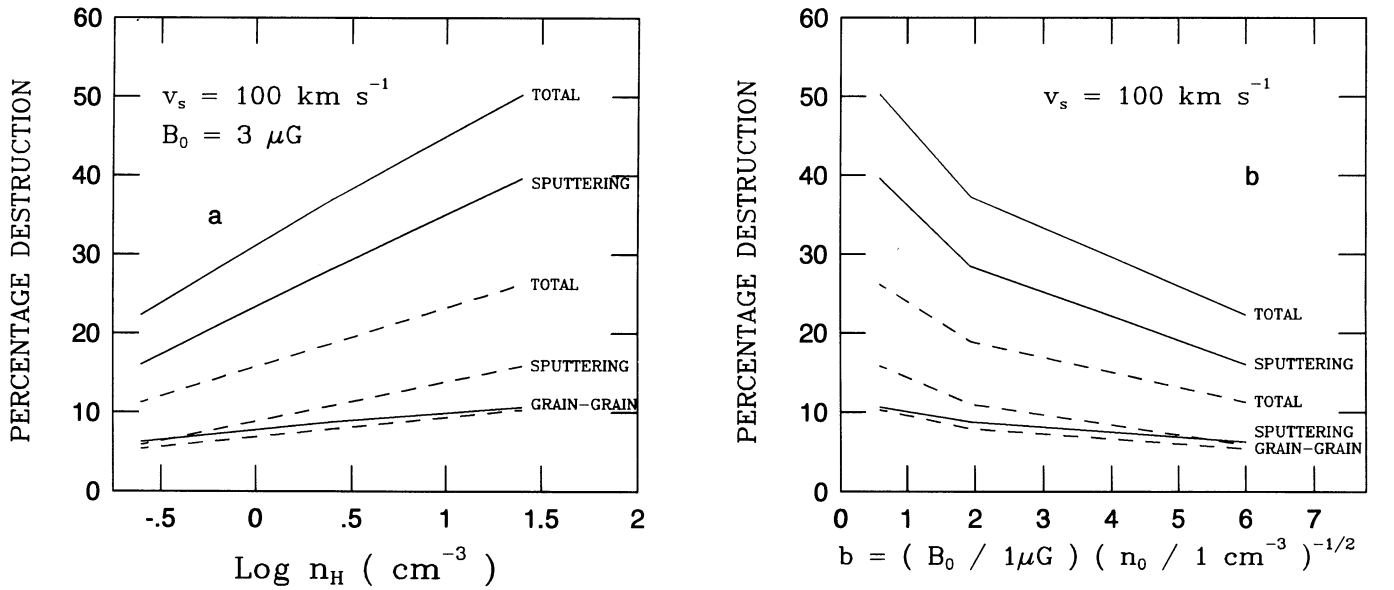

FIG. 6.—(*a*) Postshock silicate (*solid*) and graphite (*dashed*) grain destruction as a function of preshock density and destructive process (grain-grain collisions and nonthermal sputtering) for fixed shock velocity (v_s = 100 km s^{-1}) and magnetic field (B_0 = 3 μG). (*b*) Postshock silicate (*solid*) and graphite (*dashed*) grain destruction as a function of the parameter $b = B_0 n_0^{-1/2}$ and destructive process for fixed shock velocity (v_s = 100 km s^{-1}).

sooner (as measured in flow time or in column density of shocked gas) because the shocked WIM lacks the efficient cooling of the shocked WNM due to collisional excitation of Lyα and collisional ionization of hydrogen. In the WNM case, the grains undergo more betatron acceleration than in the WIM shock and therefore experience a greater degree of destruction. This effect is most marked for the smallest grains ($a < 500$ Å). However, overall the effect is small, $\leq 30\%$ (Table 2). High-velocity shocks completely ionize the gas, and hence preionization plays no role.

In our calculations we have monitored the mass in the initially empty, extra bin which represents the mass in grains of radius 40–50 Å and find that the mass deposited into and retained by this bin is very small ($< 5 \times 10^{-5}$ of the original grain mass) in our computational scheme. Grains "flowing into" this bin are subject to the destructive processes of sputtering and vaporization. Thus, sputtering and vaporization alone are unlikely to form significant numbers of small grain fragments (e.g., polycyclic aromatic hydrocarbons [PAHs] or the co-called, but ill-defined very small grains [VSGs]; Désert, Boulanger, & Puget 1990). We are currently investigating the effects of grain shattering in grain-grain collisions, an important mass redistribution process that is likely to form significant numbers of small grains.

5. TEST PARTICLES AND POROUS GRAINS

We have undertaken a test particle study in which we follow the destruction of individual grains of a particular radius through the shock profiles defined by the parameters in Table 1. These test particles are vaporized by collisions with the size distribution of graphite and silicate grains and are subject to thermal and nonthermal sputtering, but their presence does not affect the destruction of the graphite and silicate grains. Moreover, they do not collide among themselves. In addition to graphite and silicate test particles, we have also considered silicon carbide, iron, and ice particles. We have also extended this investigation to include the effects of porous/fractal grains by considering lower specific mass density grain materials.

5.1. *Homogeneous Test Particles*

The results for solid homogeneous grains are shown in Figure 7, where we have followed the destruction of 1000 Å test particles through shocks of velocity 50 km s^{-1} to 200 km s^{-1}. Clearly, silicon carbide grains, of intermediate resilience, can coexist in the interstellar medium with graphite and silicate grains. However, ice particles are easily destroyed in low-velocity shocks. The test particle data also reveal very significant destruction for iron particles, i.e., $> 70\%$ in fast shocks. This large level of grain destruction arises from the high mass density of iron and the resultant large postshock iron grain velocities (see § 2 for a discussion on this point). The iron grain velocities are in fact of order 15%–35% higher than the equivalent silicate grain velocities for 100 km s^{-1} $\leq v_s \leq$ 150 km s^{-1}.

5.2. *Porous Grains*

It has been suggested that interstellar grains are composites consisting of several types and sizes of subgrains (Mathis & Whiffen 1989). Such porous particles, with low effective specific mass densities (i.e., large ratios of surface area to volume), will behave very differently in interstellar shocks because the deceleration produced by the drag acting on the grains varies as $(a\rho_{gr})^{-1}$. Thus, low-density porous grains will not be betatron accelerated and will therefore undergo less destruction than solid homogeneous particles.

In order to simplistically model the effects of porosity on the destruction of grains, we have run the test particle calculation for the same grain types and masses, but with enhanced grain radii and reduced grain specific mass density. Thus, although we consider solid, homogeneous, and spherical particles in the calculation, we use radii and densities appropriate to large porous aggregates. Let a_s be the radius of a solid (nonporous) grain and ρ_s its mass density. If the same grain is filled with holes and inflated to a radius a, then the volume-filling factor of the solid material is given by

$$\Phi_V = \frac{a_s^3}{a^3}, \quad (1)$$

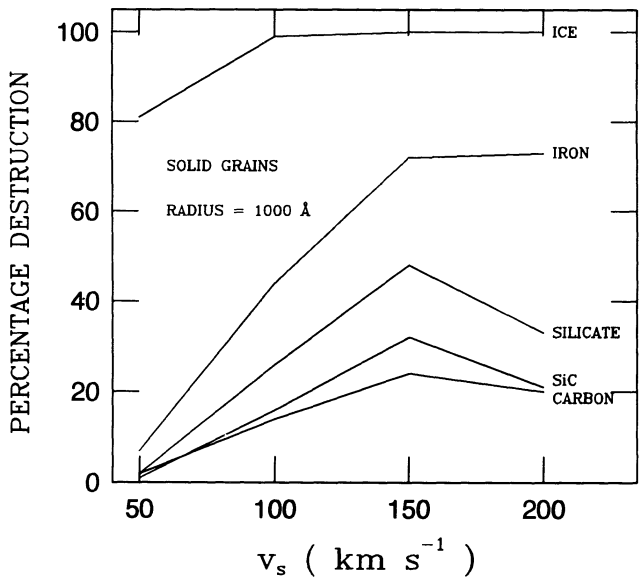

FIG. 7.—Test particle (a = 1000 Å) percentage destruction (by mass) as a function of shock velocity.

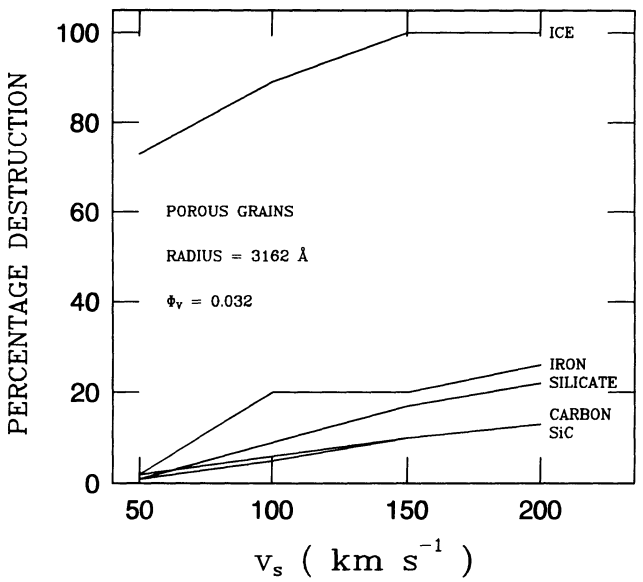

FIG. 8.—Porous particle (a = 3162 Å) percentage destruction (by mass) as a function of shock velocity.

and the mean density of this porous grain is then

$$\rho = \rho_s \Phi_V \, . \tag{2}$$

We have calculated the destruction of porous grains with $\Phi_V = 10^{-1.5}$ and $a_s = 1000$ Å ($a = 3162$ Å) and present the results in Figure 8. For particles, other than ice, there is a dramatic reduction in the level of grain destruction, as a comparison of Figures 7 and 8 clearly indicates. The destruction is reduced by as much as a factor of 3. This reduction is due to the fact that none of the particles undergo postshock betatron acceleration in any of the shocks considered. The relative gas-grain velocities are therefore always $<(3/4)v_s$, and the grains merely undergo collisional and plasma drag deceleration in the postshock phase.

It must also be pointed out that grain-grain collisions involving porous grains will lead to significant shattering of the grains, and this is something that we have not considered here but will address in a future paper.

6. GRAIN LIFETIMES

The timescale for supernova shock waves to destroy interstellar dust, $t_{\rm SNR}$, can be estimated after the method of McKee (1989); i.e.,

$$t_{\rm SNR} = \frac{M_{\rm ISM}}{(1/\tau'_{\rm SN}) \int \epsilon(v_s) dM_s(v_s)} \, , \tag{3}$$

where $M_{\rm ISM} = 4.5 \times 10^9 \, M_\odot$ is the mass of the interstellar medium (gas and dust); $\tau'_{\rm SN} = 125$ yr is the effective interval between supernovae (McKee 1989); $\epsilon(v_s)$ is the efficiency of grain destruction by a shock of velocity v_s, and M_s is the mass of gas shocked to at least v_s by a supernova remnant in the Sedov-Taylor stage—in this stage, energy is conserved so that $M_s v_s^2 \propto E$. In a three-phase model of the interstellar medium (McKee & Ostriker 1977) with a ratio of warm to hot intercloud medium filling factor of $f_w/f_h = 0.3/0.7 = 0.43$, we have

$$M_s(v_s) = 2914 \, M_\odot / v_{s7}^2 \, , \tag{4}$$

$$t_{\rm SNR} = \frac{9.7 \times 10^7}{\int \epsilon(v_{s7}) / v_{s7}^3 \, dv_{s7}} \, \text{yr} \, , \tag{5}$$

where we have assumed a mean supernova energy of 10^{51} erg.

From our calculated grain destruction data (§ 4) we have derived analytical expressions for $\epsilon(v_{s7})$ for graphite and silicate grains (radii 100 Å and 2500 Å, and the MRN distribution) for $v_{s7} = 0.5$–3. For the 100 Å grains, these fits are power laws, and for the large grains and the power-law distributions, we use linear fits to the data (Table 4). These simple analytical fits are good to within a factor of 2, in the worst case, and generally reproduce the calculated data (Table 2) to within $\pm 15\%$. In the case of 2500 Å grains we assume constant grain destruction at the highest shock velocities ($v_{s7} \geq 1.5$), 0.40 for graphite and 0.66 for silicate. We have folded the calculated $\epsilon(v_{s7})$ for graphite and silicate grains (radii 100 Å and 2500 Å, and the MRN distribution) with the shock frequency distribution ($v_{s7} = 0.5$–3), and we find grain lifetimes for the MRN power-law distributions of $t_{\rm SNR} = 4 \times 10^8$ yr and 2.2×10^8 yr for graphite and silicate, respectively. For the large grains ($a = 2500$ Å) we find lifetimes almost exactly the same as for the MRN distributions. The timescale for the power law is essentially the same as that for the large grains because of the mass is concentrated in the large grains for the MRN distribution. For the small grains ($a = 100$ Å) the lifetimes are increased by a factor of ≈ 2.5 compared to the large grains.

It is generally assumed that refractory grains are produced in stars (including supernovae; Gehrz 1989). In order to deter-

TABLE 4

GRAIN DESTRUCTION ANALYTICAL FIT PARAMETERS

		Parameter				
Grain	Size	a	b	c	d	k
Graphite.....	100 Å	0.04	3.00	...	...	...
	2500 Å	...	...	0.37	0.16	0.40
	MRN	...	...	0.19	0.08	...
Silicate.....	100 Å	0.06	3.08	...	...	...
	2500 Å	...	...	0.62	0.27	0.66
	MRN	...	...	0.37	0.17	...
	$\epsilon(v_{s7}) = a v_{s7}^b$		$0.5 \leq v_{s7} \leq 3$		100 Å	
	$\epsilon(v_{s7}) = c v_{s7} - d$		$0.5 \leq v_{s7} \leq 3$		MRN	
			$0.5 \leq v_{s7} \leq 1.5$		2500 Å	
	$\epsilon(v_{s7}) = k$		$1.5 \leq v_{s7} \leq 3$		2500 Å	

mine the equilibrium fraction of the elements locked up in refractory grains in the interstellar medium, δ_{eq}, we use equation (4) from McKee (1989), i.e.,

$$\delta_{eq} = \delta_{in}\left[1 + \frac{t_{in}}{t_{SNR}} + (\alpha - t)\frac{t_{in}}{t_{sf}}\right]^{-1}, \quad (6)$$

where δ_{in} is the dust fraction in the material injected into the interstellar medium from stellar sources; t_{in} is the timescale for the injection of refractory elements into the interstellar medium by mass loss from evolved stars and newly synthesized matter from supernovae; α is the fraction of the dust destroyed during star formation (relative to δ_{in}), i.e., $\alpha > 1$ corresponds to a net destruction of dust near the newly formed star, and $\alpha < 1$ corresponds to the net formation of dust in the protostellar environment; and t_{sf} is the star formation time. In order to simplify equation (6) we set $\alpha = 1$. Taking into account the mass injection by O and B stars which do not form dust (Jura 1987), we assume a refractory element incorporation efficiency into dust of $\delta_{in} = 0.9$. This is a very generous estimate, considering that a significant fraction of supernova ejecta is heated to X-ray–emitting temperatures. Assuming efficient dust formation in supernovae, the injection rate t_{in} is 2.5×10^9 yr (Jones & Tielens 1994). Therefore, from equation (6), the maximum fraction of the refractory elements in stardust are ≤ 0.12 for graphite and ≤ 0.07 for silicate. These values are considerably less than the observationally determined elemental depletions for dust in the diffuse interstellar medium. Observations show that the fractions of carbon and silicon in interstellar dust are ≥ 0.3 and 0.9, respectively (Mathis 1990). Observations of the 2175 Å bump and the 9.7 μm absorption feature indicate that at least 15% of the carbon is in graphitic dust and $\sim 90\%$ of the silicon is in silicate dust (Tielens et al. 1994a). Even if we assume that all the carbon is injected into the interstellar medium in the form of small (≤ 100 Å) grains, our calculated carbon stardust fraction is still not in agreement with the observed value. Moreover, only about 20% of the elemental carbon is initially injected in the form of carbon dust (Tielens 1990). The remainder is in the form of gaseous CO (C-rich and O-rich red giants), and elemental carbon (O stars and WC stars). Hence, on the average, the fraction of elemental carbon in stardust is at most 0.1, considerably less than the observations show. Due to the shorter lifetime and the observed higher fraction of silicon in dust, this discrepancy between observation and theory is even larger for silicon. To preserve a 0.9 fraction in stellar-ejected silicates, for example, requires $t_{SNR} \geq 2 \times 10^{10}$ yr, a factor 50–100 times larger than we calculate.

From our test particle calculations (§ 5), we conclude that ice particles are completely destroyed in shocks with velocities, $v_s \geq 100$ km s^{-1}, and that the lifetime for 1000 Å ice grains in the interstellar medium is $\approx 10^6$ yr. This is of the same order as the time interval between shocks of a few tens of kilometers per second. This survival time, under warm intercloud medium conditions, may be sufficient to photolyze any ice mantles, if present, to refractory organic or carbonaceous materials which may make the grains more resistant to destruction in shocks. The appropriate physical properties for the organic refractory material are not available, and this last point must remain somewhat conjectural. Photolysis may also incorporate more "refractory" carbon into the grains.

Iron particle lifetimes in the interstellar medium are also relatively short, of the order 10^8 yr, if they exist as small solid grains. This lifetime is a factor of 2 smaller than that of silicates, and the iron grain abundance in the interstellar medium will be concominantly reduced by a factor of 2. Thus, solid grains of pure iron, or iron/nickel alloy, are not a dominant interstellar dust component. Jones (1990) also argued for short lifetimes for pure iron grains in the interstellar medium on the grounds that grain surface reactions with gas-phase atomic oxygen would rapidly convert pure iron to its oxides. The high observed depletion of iron in the interstellar medium must therefore be due to iron in cores protected by outer mantles, or iron subgrains incorporated into porous grains of lower effective density, as indicated by our porous grain calculations (§ 5).

Using our simple porous grain calculations, we find that the lifetime of the grain materials in the solid phase may be enhanced by a factor of 3 if the grains are porous conglomerates (§ 5). However, the porous silicate grain lifetime ($\approx 7 \times 10^8$ yr) is still not sufficient to preserve more than 22% of the silicon in silicate grains.

7. GRAIN GROWTH IN THE INTERSTELLAR MEDIUM

7.1. *Growth by Accretion and Coagulation*

Dust can grow in the interstellar medium through the accretion of gas-phase species (mantles) and through intergrain coagulation. The former increases the ratio of grain density to gas density, while the latter merely builds larger grains from smaller grains. These processes require high densities ($n_H \geq 10^3$ cm^{-3}) and are therefore only important in dense, cold clouds (Chokshi, Tielens, & Hollenbach 1993). The dominant component of dense cloud grain mantles will be H_2O ice with small traces of other molecules such as CO, CH_3OH, and CH_4. This material is volatile and will not survive in this form in the warm intercloud medium (see § 5), so it therefore cannot be the source of grain growth in the interstellar medium. However, the ultraviolet processing of ice mantles in the dense cloud environment, or when the grains cycle into the warm intercloud medium, can lead to the formation of an organic refractory or carbonaceous material (Greenberg 1989; Jenniskens et al. 1993). Jenniskens et al. (1993) show that, given some generous assumptions, carbonization of ice mantles can lead to significant carbon grain growth in the interstellar medium of the order $2 \times 10^{-5}\ M_\odot$ kpc^{-2} yr^{-1}, or about a factor of 4 greater than the carbon stardust injection rate. Alternatively, a polymeric carbon/hydrogenated amorphous carbon might accrete directly onto preexisting grain cores (Jones, Dudley, & Williams 1990). While the chemical details of this route to mantle formation in the presence of an overabundance of hydrogen and oxygen have not been specified, it is supposed to yield a hydrogenated amorphous carbon material in the interstellar medium. Laboratory studies show that hydrogenated amorphous carbonaceous materials do indeed form from a gas or plasma that is overabundant in hydrogen (Bubenzer et al. 1983; Angus & Hayman 1988).

Given the grain lifetimes that we have determined, and observations that show that the majority of the silicate-forming elements ($\geq 90\%$) are locked up in grains in the interstellar medium, it seems that a very efficient process for the reformation or protection of silicate grains in the interstellar medium must exist. There is now some experimental evidence for a silicate formation route in the interstellar medium through SiH_n chemistry (Nuth & Moore 1988). Thus, inhomogeneous condensation routes have been proposed for both carbon and silicate grains forming from a gas of approximate

cosmic abundance composition, and also for the adsorption of a gas onto preexisting grains as mantles and subsequent ultraviolet processing. However, these routes have yet to be clearly demonstrated through detailed chemical modeling of the gas in dense and cold interstellar clouds. Under the generally accepted premise that accretion from the cold gas is indiscriminate, it is, however, very difficult to explain the (at least) bimodal interstellar grain composition if grains grow in situ in the cold interstellar medium. An attractive alternative explanation for the high silicate dust abundances observed in the interstellar medium may be that the silicate grains are protected against sputtering by carbonaceous grain mantles that can re-form on timescales much shorter than the destruction timescale, i.e., $\ll 5 \times 10^8$ yr (Liffman & Clayton 1989). We examine the protective mantle scenario in § 7.2.

Silicate grains and graphite grains do not stick as well as icy grains, and little collisional growth (coagulation) of bare silicate and graphite grains is expected in molecular clouds (Chokshi et al. 1993). However, accreted ice mantles will promote coagulation, and this synergism between accretion and coagulation may play an important role in the reformation of large grains. The icy/silicate/graphite conglomerates will be further processed in the interstellar medium by ultraviolet photons and shocks. The ultraviolet production of organic grain mantles may actually be very important, not only in making the mantles more resistant to sputtering in shocks, but also to chemically bond the agglomerated grains across their contact surfaces. In that way, refractory carbonaceous mantles could act as a "glue" which offers some protection against shattering in shocks. This idea is also attractive because porous conglomerate grains, with low effective densities, do not undergo postshock betatron acceleration (§ 5) and are therefore more resistant to shock destruction. We now investigate whether the growth of sputtering resistant carbonaceous mantles from ice mantles in the interstellar medium can explain the observed silicon depletions.

7.2. *Carbonaceous Mantle Protection of Silicate Grains*

Let us assume that carbonaceous mantles can form on silicate grains in the interstellar medium, but for the present ignore the exact mechanism of mantle formation. Recall that the grains are continually cycling between the warm medium and the cold medium. In a single cycle, they spend 3×10^6 yr in the warm medium and 3×10^7 yr in the cold medium. Under the most optimistic scenario, all of the gas-phase carbon and silicon is accreted as a refractory mantle onto the grains in a single sojourn in the cold medium. Such a mantle, on a MRN distribution of grains, would be ~ 100 Å thick and would indeed significantly increase the lifetime of the core against *sputtering*, since typically $\Delta a \sim 30$ Å is sputtered from a mantle during the 3×10^6 yr in the warm medium. However, for a given grain, the vaporization by grain-grain collisions is dominated by collisions with grains of a similar, but somewhat smaller mass. Such collisions are so destructive that both mantle and core are, at least, partially vaporized. Therefore, the lifetime of a core against grain-grain collisions is not significantly affected by a ≤ 100 Å mantle. The upper limit on the lifetime of a mantled core is therefore the grain-grain destruction lifetime. Inspection of Figure 5*a* shows that for solid grains, the grain-grain collision lifetime is ≤ 3–4 times the lifetime against both sputtering and grain-grain collisions, or $\leq 10^9$ yr. This lifetime is sufficiently short that ≤ 0.25 of the *stellar-ejected* silicates would survive in the interstellar medium, in contradiction to the ~ 0.9 for the observed silicate 9.7 μm feature. Mantles alone cannot protect stellar-ejected grains sufficiently to explain the observations.

In principle, the combination of porosity and mantle growth may increase the survival times of silicate grain cores. However, greater porosity results in a thinner mantle of adsorbed material. In addition, for very porous grains, the accreted mantles will fill the voids, thereby decreasing the porosity and increasing the material density of the grains. We reserve a detailed study of this synergism to a subsequent paper in which we shall include shattering and coagulation.

8. CONCLUSIONS

Grains are destroyed in high-velocity ($v_s \geq 150$ km s^{-1}) interstellar shock waves through thermal sputtering by high-temperature hydrogen and helium atoms/ions, and in all shocks by nonthermal sputtering and grain-grain collisions driven by the betatron acceleration of the grains. The rate of grain destruction is determined by the velocity of the grains with respect to the gas and by the time-dependent density and temperature of the postshock gas. Our treatment of the destruction of grains in shocks has incorporated several improvements and refinements over earlier work in this field (Draine & Salpeter 1979a, b; Seab & Shull 1983; McKee et al. 1987), including updated sputtering yields based on laboratory data and the treatment of partial vaporization of grains in grain-grain collisions.

We find that the destruction of grains in grain-grain collisions is less important than has previously been assumed (Seab & Shull 1983; McKee et al. 1987) and, consequently, that the destruction of grains in interstellar shocks is dominated by nonthermal and thermal sputtering. However, because the sputtering yields used here are higher, particularly at the lower relative velocities, we find that the degree of grain destruction is similar to that calculated by McKee et al. (1987). Since, somewhat more than in previous models, sputtering dominates grain-grain collisions, the cores of the refractory grains can be preserved. Thus, the isotopic compositions of the grain-forming environments can be preserved in the grain cores. Also, ice mantles rapidly form in dense clouds, and isotopic fractionation occurs; this will be carried into protosctellar disks if the ices survive the infall.

It should be pointed out that our results almost certainly underestimate the destruction of large grains because we ignore the effects of shattering. The threshold pressure for shattering is of order 100 kbar and considerably lower than that for vaporization, which is ≈ 5 Mbar. Therefore grain-grain collisions will shatter large grains into smaller fragments and considerably reduce the large-grain concentrations. We have also ignored the pressure drop effects in blast waves and thus have overestimated the grain destruction. The inclusion of this effect could reduce the destruction by a factor of 1.5–2 in Sedov-Taylor blast waves and by a smaller factor in evaporative blast waves (McKee et al. 1987).

We conclude that a considerable fraction of solid homogeneous interstellar dust grains are relatively easily destroyed in the warm interstellar medium in supernova blast waves. The lifetime of this dust is of the order of 4×10^8 yr for graphite grains and 2.2×10^8 yr for silicate dust. Both timescales are shorter than the stardust injection timescale of 2.5×10^9 yr and imply that only a relatively small fraction of the heavy elements can be tied up in dust created in stars, i.e., ≤ 0.12 for

carbon and ≤ 0.07 for the silicate-forming elements. Therefore, dust must efficiently condense in the interstellar medium, presumably in the form of refractory mantles on existing grains.

Silicon carbide grains can survive in the interstellar medium as well as carbon grains; i.e., their lifetimes against destruction are similar. However, we find that iron grains are not likely to be an important component of interstellar dust because they undergo rapid destruction in fast shocks. Not surprisingly, we find that volatile ice mantles do not survive in the warm intercloud medium. One shock of velocity ≥ 50 km s^{-1} is sufficient to destroy $\geq 80\%$ of a 1000 Å ice layer. However, ultraviolet processing of icy mantles may result in refractory mantles, which will protect their cores against sputtering, and can therefore protect stellar-ejected dust.

If the silicate grains can be protected by mantles, and if substantial refractory mantles can reform in the interstellar medium on appropriate timescales, i.e., 3×10^7 yr in a dense cloud, then dust destruction will be dominated by grain-grain collisions. In that case, the grain lifetime is enhanced by a factor of ~ 3–4. Similarly, if the grain s are porous, the lifetime may be enhanced by a factor of ~ 3. Therefore, in either case, only $\leq 25\%$ of the stellar-produced silicates can be preserved in the dust. This enhanced silicate grain lifetime is $t_{\rm SNR} \approx 10^9$ yr and is a factor of ≈ 20 smaller than that required to preserve 90% of the (stellar-produced) silicates in the diffuse interstellar medium ($t_{\rm SNR} \geq 2 \times 10^{10}$ yr).

We concluded by summarizing the possible scenarios that are consistent with observational constraints and the dust destruction model presented in this paper:

1. Most (90%) of the silicon exists in silicates. Significant destruction of stardust occurs in the interstellar medium, and most of the silicate is formed in the interstellar medium. Little ($\leq 7\%$) stardust survives as interstellar dust.
2. Most (90%) of the silicon exists in silicates. There is no significant silicate formation in the interstellar medium. However, the supernova shock frequency in the warm medium, or the cycling frequency from the warm medium to the cold medium, is much less (by a factor of ~ 100) than the generally accepted values. The silicates are preserved stardust.
3. The 9.7 μm absorption measurements do not sample average interstellar material. Only a small fraction (perhaps 20%) of silicon is in interstellar silicate dust grains. This stellar-ejected silicate is protected by refractory mantles and possibly porosity. The remainder of the depleted silicon is in this (nonsilicate) mantle.

We are greatly indebted to J. Raymond for his time spent generating the shock profiles that we have used in this study. We wish to thank the referee for many helpful comments and suggestions. Funds for the support of this study have been allocated by the NASA-Ames Research Center, Moffett Field, California, under Interchange NCA 2-637. Theoretical studies of interstellar dust at NASA Ames are supported through NASA grant 399-29-01-30 from the Astrophysics Theory Program.

APPENDIX A

OUTLINE OF THE COMPUTATIONAL METHOD

The basis of the method, as applied to grain coagulation in accretion disks, is to be found in Nakagawa et al. (1981) and Mizuno et al. (1988). We have adapted this method to erosional rather than growth processes. The form used here as applied to the processes of grain-grain collisions (vaporization) and sputtering (thermal and nonthermal) is given below.

The rate of change of number density of particles in the mass range m to $m + dm$ is given by

$$\frac{\partial}{\partial t} n(m, t) = -n(m, t) \int_{m-}^{m+} n(m_i, t)\alpha'(m, m_i, v)dm_i - \frac{\partial}{\partial m} n(m, t)\dot{m}_{\rm sp}(m, v) + \frac{1}{2} \int_{m-}^{m+} \int_{m-}^{m+} n(m_i, t)n(m_j, t)\alpha'(m_i, m_j, v)P_{ij}\, dm_i\, dm_j + \int_{m-}^{m+} n(m_i, t) \frac{\dot{m}_{\rm sp}(m_i, v)}{m_i}\, dm\,, \quad \text{(A1)}$$

$$\alpha'(m_i, m_j, v) = \sigma(m_i, m_j)v(m_i, m_j)\,, \quad \text{(A2)}$$

where the first and second terms in equation (A1) are the collisional vaporization and the sputtering loss terms, and the third and fourth terms are the respective gain terms. $\dot{m}_{\rm sp}(m_i)$ is the mass ablation rate due to sputtering, $\sigma(m_i, m_j)$ is the grain-grain collision cross section, and $v(m_i, m_j)$ is the relative collision velocity. The relative velocity is calculated by summation over the respective grain velocity vectors for each of the colliding grains, i.e.,

$$v(m_i, m_j) = \tfrac{1}{4}\{[v(m_i) + v(m_j)] + [|\, v(m_i) - v(m_j)\,|] + [v(m_i)] + [v(m_j)]\}\,. \quad \text{(A3)}$$

In the case of grain-grain collisions the fractional vaporization is calculated at each of the four velocities in the square brackets on the right-hand side of equation (A3) and then summed with equal weight (0.25) to give the integrated fractional vaporization for each collision [for $v(m_i) > 0$ and $v(m_j) > 0$]. If either grain velocity is zero then the relative velocity is set equal to the nonzero velocity, and where both grain velocities are zero no collisions occur. For sputtering processes the relevant velocity is simply that of the grain under consideration. P_{ij} is a resultant mass switch, $P_{ij} = 1$ if the collision of grains of masses m_i and m_j yields a fragment in the mass range m to $m + dm$, otherwise $P_{ij} = 0$. In the above, and hereafter, we have combined the thermal and nonthermal sputtering terms for simplicity; in the full calculation these two sputtering processes are treated separately through an equivalent and independent sets of terms. We have here only included the effects of particles of the same composition colliding, again for the sake of simplicity.

Defining $\rho(m, t) = mn(m, t)$ and $\alpha(m_i, m_j, v) = \alpha'(m_i, m_j, v)/m_i m_j$, we can write the scheme in a form that strictly guarantees the conservation of mass (Mizuno et al. 1988). Then

$$\frac{\partial}{\partial t}\rho(m, t) = -m\rho(m, t)\int_{m-}^{m+}\rho(m_i, t)\alpha(m, m_i, v)dm_i - \frac{\partial}{\partial m}\rho(m, t)\dot{m}_{sp}(m, v) + \frac{m}{2}\int_{m-}^{m+}\int_{m-}^{m+}\rho(m_i, t)\rho(m_j, t)\alpha(m_i, m_j, v)P_{ij}dm_i dm_j + \frac{1}{m}\int_{m-}^{m+}\rho(m_i, t)\dot{m}_{sp}(m_i, v)dm_i . \quad \text{(A4)}$$

For computation, equation (A4) is discretized into z mass bins and the system of $4z$ ordinary differential equations for grain velocity and total bin mass for each grain type (graphite and silicate) is solved computationally using a Runge-Kutta scheme with adaptive step-size control (Press et al. 1990). In order to simplify the treatment of sputtering computationally we use a scheme that "removes" the grains from the bin under consideration (k), subject those grains to sputtering, and then places the sputtered grain remnants into the appropriate mass bins ($\geq k$, i.e., the same or a smaller mass bin). The discretized equations for the kth of z mass bins are therefore solved computationally in the form

$$\frac{dV_k}{dt} = \frac{d\chi}{dt}\frac{V_k}{2\chi} - \frac{F_D(\text{collision}) + F_D(\text{plasma})}{\bar{m}_k}, \quad \text{(A5)}$$

$$\frac{dM_k}{dt} = -\bar{m}_k\rho_k\delta_k\sum_{i=1}^{z}\alpha_{ik}\rho_i\delta_i - \rho_k\delta_k + \sum_{i=1}^{k}\sum_{j=1}^{z}\alpha_{ij}\rho_i\delta_i\rho_j\delta_j m_i(k) + \sum_{i=1}^{k}\rho_i\delta_i\frac{m_{i,sr}(k)}{\bar{m}_i}, \quad \text{(A6)}$$

where V_k is the velocity of the grains in the kth bin, χ is the compression behind the shock, F_D(collision) and F_D(plasma) are the collisional and plasma drag terms (McKee et al. 1987), $\rho_k = \bar{m}_k n(\bar{m}_k)$ is the kth bin particle mass density term, $\bar{m}_k$ is the mean bin mass, and δ_k is the bin width. $m_i(k)$ is the resultant mass of the ith particle in the collision of ith and jth particles that lies within the mass bounds of the kth bin, and similarly $m_{i,sr}(k)$ is the resultant ith particle sputtered mass that lies within the mass bounds of the kth bin.

The power-law index for each mass bin, the local power law, β_k, is determined after the method of Mizuno et al. (1988), with the exception that the extreme mass bin indices are determined using only two adjacent bins rather than the usual three. The derived power-law index for each bin is used to calculate the mean grain masses for each bin; thus,

$$\bar{m}_k = \frac{(1-\beta_k)}{(2-\beta_k)}\frac{(1-\eta^{2-\beta_k})}{(1-\eta^{1-\beta_k})}m_{k+}, \quad \text{(A7)}$$

where m_{k+} is the upper mass limit to the kth bin.

APPENDIX B

THE PRESSURE DROP IN SEDOV-TAYLOR BLAST WAVES

Grain destruction can be reduced by the pressure drop that occurs behind an expanding blast wave (McKee et al. 1987). The pressure drop decreases the temperature of the gas and tends to reduce the density and magnetic field. Since radiative losses also reduce the temperature but tend to increase the density and magnetic field, the pressure drop becomes important only when it occurs on a timescale less than or of the order of the cooling time—i.e., at high shock velocities. When the pressure drop is significant, the decrease in magnetic field can result in betatron deceleration of the grains, substantially reducing nonthermal sputtering.

We illustrate the pressure drop effect for the 200 km s^{-1} case. By neglecting the effects of radiative losses, we obtain a lower limit on the magnetic field behind the shock and thus a lower limit on the amount of grain destruction. McKee et al. (1987) treated the case of shocked clouds; here we consider a Sedov-Taylor blast wave propagating in a warm intercloud medium. Let R_b be the radius of the blast wave at time t and let $\lambda \equiv r/R_b$ be the similarity variable. The mass inside r is denoted by $M(r)$. Let $\rho_1(t)$ and $P_1(t)$ be the density and pressure just behind the blast-wave shock (we have dropped the subscript i used by McKee et al. for simplicity). Using the linear pressure approximation of Gaffet (1978), or equivalently, the pressure gradient approximation of Ostriker & McKee (1988), one finds

$$\tilde{\rho} \equiv \frac{\rho(r)}{\rho_1} \simeq \lambda^9, \quad \text{(B1)}$$

$$\tilde{M} \equiv \frac{M(r)}{M(R_b)} \simeq \lambda^{12}, \quad \text{(B2)}$$

$$\tilde{P} \equiv \frac{P(r)}{P_1} \simeq \frac{1+2\lambda^{12}}{3} \simeq \frac{1+2\tilde{M}}{3}. \quad \text{(B3)}$$

Consider an element of gas which is shocked at a time t_0, when the blast wave has a velocity v_{b0}. The pressure of the gas at time t, as compared to its initial postshock value, is

$$\frac{P(t)}{P_1(t_0)} = \frac{P(t)}{P_1(t)} \cdot \frac{P_1(t)}{P_1(t_0)} = \tilde{P}\left[\frac{R_b(t_0)}{R_b(t)}\right]^3 = \frac{(1 + 2\tilde{M})\tilde{M}}{3} . \tag{B4}$$

Since the expansion is adiabatic, the density is $\rho(t)/\rho_1(t_0) = [P(t)/P_1(t_0)]^{3/5}$, and correspondingly, the temperature is $T(t)/T_1(t_0) = [P(t)/P_1(t_0)]^{2/5}$. To express these results in terms of time, we note that since a Sedov-Taylor blast wave in a uniform medium expands as $R_b \propto t^{2/5}$, its Lagrangian mass coordinate is

$$\tilde{M} = \left[\frac{R_b(t_0)}{R_b(t)}\right]^3 = \left(\frac{t_0}{t}\right)^{6/5} \qquad (t \geq t_0) . \tag{B5}$$

Numerically, we have

$$t_0 = 4.46 \times 10^{12}\left(\frac{E_{51}}{n_0}\right)^{1/3} v_{b0,7}^{-5/3} \text{ s} \tag{B6}$$

for a Sedov-Taylor blast wave, where E_{51} is the supernova energy in units of 10^{51} erg. Equations (B4)–(B6) provide an explicit expression for the time evolution of the pressure of an element of gas hit by a shock of velocity v_{b0}.

REFERENCES

Allen, C. W. 1983, Astrophysical Quantities (London: Athlone)
Angus, J. C., & Hayman, C. C. 1988, Science, 241, 913
Barlow, M. J. 1978a, MNRAS, 183, 367
———. 1978b, MNRAS, 183, 397
Bubenzer, A., Dischler, B., Brandt, G., & Koidl, P. 1983, J. Appl. Phys., 54, 4590
Chokshi, A., Tielens, A. G. G. M., & Hollenbach, D. 1993, ApJ, 806
Cowie, L. L. 1978, ApJ, 225, 887
Désert, F. X., Boulanger, F., & Puget, J. L. 1990, A&A, 237, 215
Draine, B. T., & Lee, H. K. 1984, ApJ, 285, 89
Draine, B. T., & Salpeter, E. E. 1979a, ApJ, 231, 77
———. 1979b, ApJ, 231, 438
Dwek, E., & Scalo, J. M. 1980, ApJ, 239, 193
Gaffet, B. 1978, ApJ, 225, 442
Gehrz, R. D. 1989, in Interstellar Dust, ed. L. J. Allamandola & A. G. G. M. Tielens (Dordrecht: Kluwer), 445
Greenberg, J. M. 1989, in Interstellar Dust, ed. L. J. Allamandola & A. G. G. M. Tielens (Dordrecht: Kluwer), 345
Hollenbach, D., & McKee, C. F. 1979, ApJS, 41, 555
Jenniskens, P., Baratta, G. A., Kouchi, A., de Groot, M. S., Greenberg, J. M., & Strazzulla, G. 1993, A&A, 273, 583
Jones, A. P. 1990, MNRAS, 245, 331
Jones, A. P., Duley, W. W., & Williams, D. A. 1990, QJRAS, 31, 567
Jones, A. P., & Tielens, A. G. G. M. 1994, in The Cold Universe, XIIIth Moriond Astrophysics Meeting, ed. T. Montmerle, C. J. Lada, I. F. Mirabel, & J. Tran Thanh Van (Gif-sur Yvette: Editions Frontieres), 35
Jura, M. 1987, in Interstellar Processes, ed. D. J. Hollenbach & H. A. Thronson, Jr. (Dordrecht: Reidel), 3
Liffman, K., & Clayton, D. D. 1989, ApJ, 340, 853
McKee, C. F. 1989, in Interstellar Dust, ed. L. J. Allamandola & A. G. G. M. Tielens (Dordrecht: Kluwer), 431
McKee, C. F., Hollenbach, D. H., Seab, C. G., & Tielens, A. G. G. M. 1987, ApJ, 318, 674
McKee, C. F., & Ostriker, J. P. 1977, ApJ, 218, 148
Mathis, J. S. 1990, ARA&A, 28, 37
Mathis, J. S., Rumpl, W., & Nordsieck, K. H. 1977, ApJ, 217, 105 (MRN)
Mathis, J. S., & Whiffen, G. 1989, ApJ, 341, 808
Mizuno, H., Markiewicz, W. J., & Völk, H. J. 1988, A&A, 195, 183
Nakagawa, Y., Nakagawa, K., & Hayashi, C. 1981, Icarus, 45, 517
Nuth, J. A., & Moore, M. A. 1988, ApJ, 329, L113
Ostriker, J. P., & McKee, C. F. 1988, Rev. Mod. Phys., 60, 1
Press, W. H., Flannery, B. P., Teukolsky, S. A., & Vetterling, W. T. 1990, Numerical Recipes (Cambridge: Cambridge Univ. Press)
Raymond, J. 1992, private communication
Routly, P. M., & Spitzer, L. 1952, ApJ, 115, 227
Seab, C. G. 1987, in Interstellar Processes, ed. D. J. Hollenbach & H. A. Thronson, Jr. (Dordrecht: Reidel), 491
Seab, C. G., & Shull, J. M. 1983, ApJ, 275, 652
Tielens, A. G. G. M. 1990, in Carbon in the Galaxy, ed. J. C. Tarter, S. Chang, & D. De Frees (NASA CP 3061), 59
Tielens, A. G. G. M., Allamandola, L. J., Bregman, J., & Witteborn, F. C. 1994a, in preparation
Tielens, A. G. G. M., McKee, C. F., Seab, C. G., & Hollenbach, D. H. 1994b, ApJ, 431, 321